Iranian Journal of Materials Forming 12 (2) (2025) 58-67

Online ISSN: 2383-0042

IJMF

Iranian Journal of Materials Forming

Journal Homepage: http://ijmf.shirazu.ac.ir

Research Article

Effect of Constrained Groove Pressing on Anisotropy and Formability of Al-1050: Insights from Forming Limit Diagrams

A. Motallebi[1], V. Alimirzaloo[1*] and M. Gerdooei[2]

[1] Department of Mechanical Engineering, Faculty of Engineering, Urmia University, Urmia, Iran
[2] Faculty of Mechanical and Mechatronics Engineering, Shahrood University of Technology, Shahrood, Iran

ARTICLE INFO

Article history:

Received 5 March 2025
Reviewed 23 April 2025
Revised 15 May 2025
Accepted 19 May 2025

Keywords:

CGP
FLD
Formability
Elongation
Tensile strength

Please cite this article as:

Motallebi, A., Alimirzaloo, V., & Gerdooei, M. (2025). Effect of constrained groove pressing on anisotropy and formability of Al-1050: insights from forming limit diagrams. *Iranian Journal of Materials Forming*, *12*(2), 58-67. https://doi.org/10.22099/IJMF.2025.52624.1329

ABSTRACT

Constrained groove pressing (CGP) is an effective severe plastic deformation (SPD) technique used to strengthen metals by refining their microstructure, resulting in enhanced material strength but reduced formability. The forming limit diagram (FLD) is a critical tool for representing the deformability of sheet metals under various loading conditions before necking occurs. Despite its significance, the effects of CGP parameters on FLD diagrams have not been thoroughly investigated. This study examines the influence of CGP passes on the FLD and mechanical properties of Al-1050 aluminum sheets. The results reveal that the yield strength increased from 133 MPa after the first pass to 140 MPa and 160 MPa after the second and third passes, respectively. The ultimate tensile strength (UTS) initially rose to 185 MPa after the first pass, representing a 26% improvement compared to the as-received material, but then slightly decreased by 3.9% and 4.3% after the second and third passes, respectively. Elongation exhibited a sharp 45% reduction following the first pass but improved by 18% in the second and third passes compared to the first pass. These mechanical property trends can be attributed to grain refinement, the evolution of ultra-fine grains, reduced strain hardening, and an increased rate of cell formation during the CGP process. The FLD showed a significant 50% reduction after the first pass relative to the as-received condition, but gradually increased with subsequent passes, improving by 8% and 25% after the second and third passes, respectively. Furthermore, an increase in the number of passes significantly reduced planar anisotropy variation.

1. Introduction

Investigations into materials with a high strength-to-weight ratio play a critical role in to reducing vehicle weight and, consequently, fuel consumption. Studies have shown that aluminum accounts for approximately 30% of materials used in the automotive industry, with one-third of this utilized in sheet metal forming. Research suggests that a 10% reduction in vehicle weight can lead to an 8-10% decrease in fuel consumption [1]. Despite competition from other lightweight materials such as advanced high-strength steel, magnesium alloys, and reinforced plastics, aluminum remains a preferred choice due to its favorable characteristics, including accessibility, recyclability, and

* Corresponding author
E-mail address: v.alimirzaloo@urmia.ac.ir (V. Alimirzaloo)
https://doi.org/10.22099/IJMF.2025.52624.1329

cost-effective mass production.

Severe plastic deformation (SPD) is a top-down technique used to produce nano-structured metals [2, 3]. It has evolved to enable the application of higher strain levels to materials [4-11]. Various SPD methods include equal channel angular pressing (ECAP) [2], high pressure torsion (HPT) [12], constrained equal channeling (CEC) [9], and twist extrusion (TE) [4]. For sheet metals, techniques such as accumulative roll bonding (ARB) [11], friction stir processing (FSP) [8], repetitive corrugation and straightening (RCS) [5-7], continuous gradient rolling (CGR) [6], and constrained groove pressing (CGP) [10] have been proposed.

ARB and CGP methods are known as considerable approaches for SPD of sheet metal components. The ARB method was proposed by Saito et al. [13, 14], and is achieved by repetitive bonding between metal layers. If proper bonding does not occur, the non-deformed areas cannot contribute to improving the properties. However, this limitation is not present in the CGP process (Fig. 1). This method [15] is capable of creating higher and more homogenous strain [16, 17]. During CGP operation, the deformation region appears under a pure shear stress state. Each pass consists of four stages (two bending and two flattening stages) which can impose an effective strain of up to 1.16, as illustrated in Fig. 2. Recently, various metals have been processed using the CGP technique [15, 17-19], including copper [20, 21], nickel [22], and low carbon steel [23, 24]. In the CGP process, a pair of corrugating and flattening dies is used to induce sever plastic deformation on the sheet (Fig. 1). Each pass involves four stages, two corrugating and two flattening stages (Fig. 2). By applying a 180° rotation between stages, a higher degree of uniformity in microstructural and mechanical properties can be achieved.

The forming limit diagram (FLD) is a well-known method to predict the plastic deformation limit of sheet samples. FLD can detect the limiting surface strains that sheet samples can tolerate before localized necking occurs. It shows the combinations of major and minor surface strains that result in damage of the sample. The plots for FLD can be calculated both theoretically [25] and experimentally. FLD was first proposed by Keeler Goodwin [26] to indicate defects such as necking and fracture behavior in sheet metals. Marciniak and Kuczynski [27] expanded this theory and extracted a model for predicting localized necking. They figured out that failure in sheet metal forming does not take place suddenly, but rather the inhomogeneity and heterogeneity in the constituent microstructure of the material lead to localized thinning and ultimately failure. This behavior results in a groove dividing the sheet surface into homogeneous and heterogeneous regions. Zahedi and colleagues [28] predicted the necking and fracture limit diagrams for Al-Cu two-layer sheets during the cup drawing test. They used a modified Gurson-Tvergaard damage model and a time-dependent model to predict the numerical values of the necking limit diagrams. They also experimentally demonstrated that cracks initiate and propagate from the outer layer. Alizad Kamran and Mollaei Dariani [29] investigated the capability of the BBC2008 (16 and 8 parameter) yield models and the Hill-48 yield model in extracting limit strain diagrams for sheet AA3003-H19 theoretically using the M-K model. They concluded that all three models, BBC2008 (16 and 8 parameters) and the Hill-48 yield model, predict the left side of the limit strain diagram in good agreement with experimental data. Lee and colleagues [30] conducted an accumulative roll bonding process on AA6061 for 8 cycles.

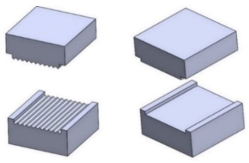

Fig. 1. Schematic representation of dies of CGP method.

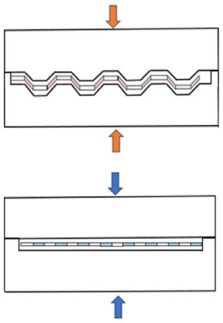

Fig. 2. Schematic representation of corrugating and flattening stages of CGP process.

The results obtained show that very fine grains with clear boundaries appear from the third cycle and encompass the entire structure in the eighth cycle. The tensile strength increases with the number of cycles, reaching 363 MPa in the eighth cycle, which is nearly three times the initial value. On the other hand, the elongation increases abruptly in the first cycle and then decreases in the subsequent cycles.

The literature suggests that mechanical processing offers a promising approach to enhancing the strength and microstructure of pure aluminum, making it a valuable material for the automotive industry. CGP, a straightforward severe plastic deformation technique, has gained significant attention for its ability to produce ultra-fine grain structures in sheet metals. Additionally, as mentioned earlier, FLDs are effective tools for analyzing the fracture behavior of sheet metals. While FLDs have been extensively studied in some SPD processes, such as ARB, a review of the existing studies reveals a notable gap regarding FLDs for CGP-processed samples. Therefore, this paper experimentally investigates the influence of the number of CGP passes on the FLD of Al-1050 aluminum sheets.

2. Experimental Procedure

The samples of 90 × 90 mm with thicknesses of 2 mm were prepared from Al-1050 rolled sheets in room temperature condition. The chemical composition of the Al-1050 was achieved by inductively coupled plasma mass spectroscopy (ICP-MS) as stated in Table 1. The ram speed of 5 mm/min was used during the process, and the dry condition was selected for the contact surface between die and sample in this study. The CGP samples were performed along the rolling direction. A schematic of the investigated sheet directions is shown in Fig. 3. After applying different passes of CGP, the resultant samples were considered for FLD operation. To extract the tensile test, the strain rate of 0.01 1/s was set by the test machine on cold condition.

Each pass of the CGP process includes four stages: according to Fig. 4, in each stage, a die with a groove angle θ = 45° imposes a shear strain value of 1:

$$\gamma_{xy} = \frac{\Delta x}{\Delta x} = \tan 45^{\circ} = 1$$

According to the von Mises criterion, the effective strain can be calculated using the following relation:

$$\varepsilon_{eff} = \sqrt{\frac{2}{9}[(\varepsilon_x - \varepsilon_y)^2 + (\varepsilon_y - \varepsilon_z)^2 + (\varepsilon_x - \varepsilon_z)^2] + \frac{4}{3}[\varepsilon_{xy}^2 + \varepsilon_{yz}^2 + \varepsilon_{zx}^2]} \quad (1)$$

By considering $\varepsilon_{xy} = \frac{\gamma_{xy}}{2}$, and the assuming pure shear during deformation with no strain along length and width $(\varepsilon_{yz} = \varepsilon_{zx} = \varepsilon_z = \varepsilon_y = \varepsilon_x = 0)$, the effective strain in each stage is:

$$\varepsilon_{eff} = \frac{1}{\sqrt{3}} = 0.58 \quad (2)$$

This strain is exerted on the sheet twice in each pass. Therefore, one pass creates an effective strain of 1.16 throughout the sheet [31]. This value is approximately constant across the entire sheet.

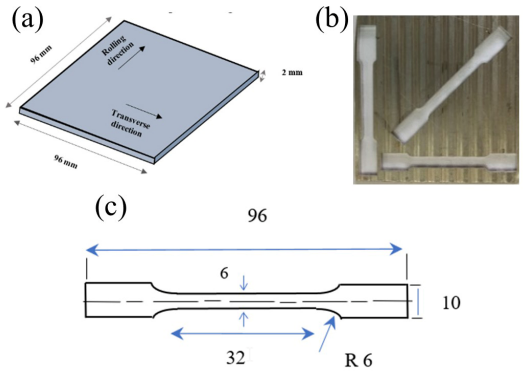

Fig. 3. (a) Rolling and transverse directions in the examined sheet samples, (b) samples extracted from processed specimen in the current study for the CGP process, and (c) dimensions of tensile test specimen (mm).

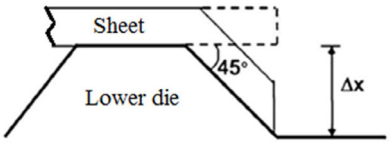

Fig. 4. Geometrical parameters of the CGP process.

Table 1. Chemical composition of Al-105 determined by ASTM E1251

Element	Al	Fe	Si	Mn	Sb	Ti	P
wt. %	98.8	0.570	0.375	0.0827	0.0284	0.0148	0.0133

By repeating this process, a very large plastic strain can be created in the specimen, and an ultrafine-grained structure can be obtained without changing the initial dimensions. Fig. 5 shows the CGP dies and equipment.

Finally, in order to investigate the fracture and obtain FLD diagrams, the FLD tests were carried out by the Nakazima test (Fig. 6) on CGPed samples of Al-1050 to develop the fracture strain. The tests were carried out for various passes of CGP process. The ram with a specific radius for FLD was designed and then manufactured. In the Nakazima test, biaxial stretch-forming tests are applied for FLDs. Various samples with different groove dimensions were used for FLD, as illustrated in Fig. 7(a). The specimens were cut by wire-cut machine from CGPed and as-received sheet samples with a diameter of 93 mm. An electro-chemical procedure was applied to create the circular grid (2.5 mm diameter and a depth of 1 micrometer) on the surface of the as-received and CGPed samples. A Santam 100-ton constant speed hydraulic press machine equipped with a displacement–force curve monitor was used to carry out the experimental tests. Typical undeformed (circular grid) and deformed (elliptical grid) samples for Nakazima test are illustrated in Fig. 7. After the test, the circular grids were deformed into elliptical geometry by the tests. Eqs. (3) and (4) were used to measure the major and minor engineering strains, respectively, and then stated in the true strain relation:

$$e_{major\,(\%)} = \frac{a-d}{d} \times 100\,,\ \varepsilon_{major} = \ln(1 + e_{major}) \qquad (3)$$

$$e_{minor\,(\%)} = \frac{b-d}{d} \times 100\,,\ \varepsilon_{minor} = \ln(1 + e_{minor}) \qquad (4)$$

a, b and d introduce the ellipse's major and minor diameters and the initial circle diameter, respectively. ε_{major} and ε_{minor} show the true major and minor strains, respectively. To obtain the specimens for tensile test, the samples were cut along RD and TD directions (Fig. 3) according to ASTM-E8M, as shown in Figs. 7(c) and 7(d). Room temperature was applied, using a constant cross-head velocity and an initial strain rate of 4×10^{-4} s^{-1}.

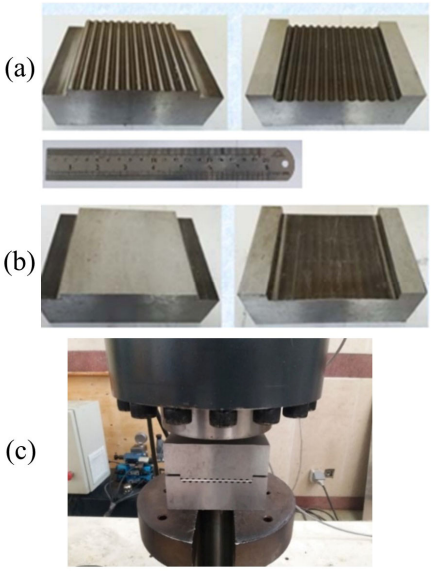

Fig. 5. CGP dies: (a) grooving die, (b) flattening dies, (c) CGP dies under press (groove angle θ = 45°, groove width = 2 mm, and die dimension = 96 × 96 mm).

Fig. 6. Nakazima FLD dies under press.

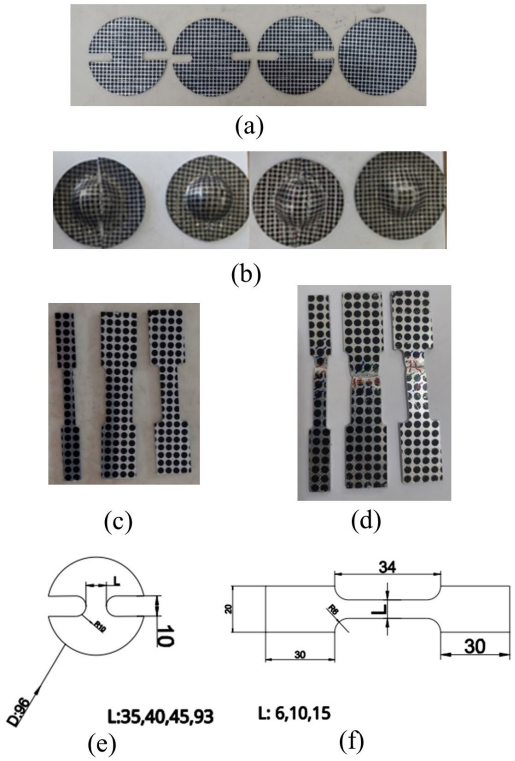

Fig. 7. Samples for FLD: Nakazima samples; (a) before the test, (b) after the test, tension samples; (c) before the test, (d) after the test, (e) dimension of tension samples, and (f) dimensions of Nakazima samples.

3. Results and Discussion

3.1. Mechanical properties

The as-received sample (Al-1050) showed the minimum yield tensile strength (YS) (118 MPa) and elongation of nearly 20%, and the ultimate tensile strength (UTS) of about 147 MPa was measured, as illustrated in Fig. 8. The results also showed that 0.2% yield strength was enhanced after the first pass of the CGP process, reaching 140 and 160 MPa for the second and third passes, respectively. Compared to the as-received sample, the ultimate tensile strength for the first pass increased to 185 MPa (with a 26% increase). However, with the rising the number of passes from one to three, the ultimate tensile strength began to decrease, dropping by 3.9% and 4.3% for the second and third passes, respectively. Dislocation accumulation and grain refinement are two major mechanisms responsible for strengthening during CGP process [32-34]. The increase in ultimate strength after the first pass is attributed to strain hardening and cold work. However, the decrease in UTS after the first pass is attributed to the combined effects of grain refinement, reduced work hardening, and strain hardening saturation. Also, the findings disclosed that for the third pass, the influence of cold working was reduced, and grain refinement was observed [35]. At higher passes, possibly due to texture evolution and the emergence of misorientated planes, condition for higher ductility with lower strength may be formed. In the first pass of CGP, the FLD region without damage was significantly reduced because of the appearance of cold work in the sample. With the increase in the number of CGP passes, this region began to grow, which can be related to the reduction of strain hardening, the break of grain boundaries and the reduction of separation of sheet layers.

The ultimate tensile strength, 0.2% yield strength, and elongation for different CGP passes and the as-received sample were obtained, as illustrated in Fig. 9. It shows that the elongation exhibits a sharp decrease after the first pass compared to as-received sample, where the maximum difference reaches up to 45%. However, the elongation improves with additional CGP passes, for the second and third passes, an improvement of about 18% is observed compared to the first pass. The enhancement in elongation after the first pass can be attributed to grain refinement, the gradual formation of ultra-fine grains, reduction in strain hardening and the higher rate of cell formation, which consequently leads to increased nucleation at grain boundaries. From the first to the third pass, the ultimate tensile strength continues to decrease, due to ongoing grain refinement and a higher recovery rate during the deformation process. However, the yield strength exhibits a steady upward trend from the as-received state to the third pass, with increases of the 13%, 18% and 36% for the first pass, second and third passes, respectively, compared to the as-received sample.

Fig. 10 shows the diagram of the number of passes versus Vickers hardness for the CGP process of Al-1050. It shows that as the number of passes rises, the hardness value increases, reaching 75 V at the third pass, showing an increase of 21, 17 and 5 V with respect to the as-received, pass 1 and pass 2 samples, respectively.

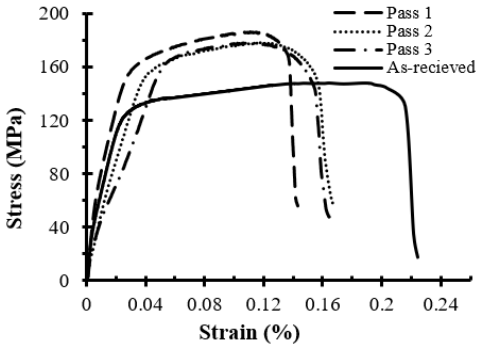

Fig. 8. True stress-strain curves for as-received and CGPed samples.

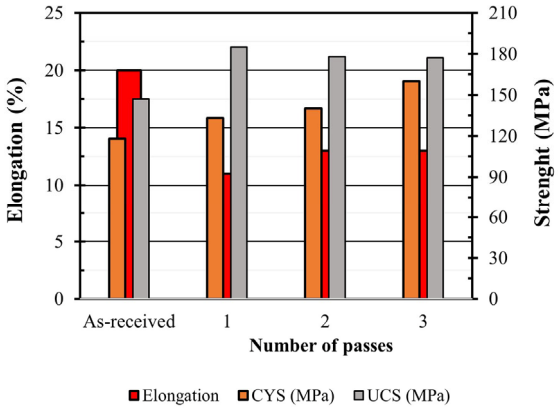

Fig. 9. Diagrams of ultimate tensile strength (UCS), yield strength (CYS), and elongation for the as-received sample and CGPed Al-1050 after different numbers of passes.

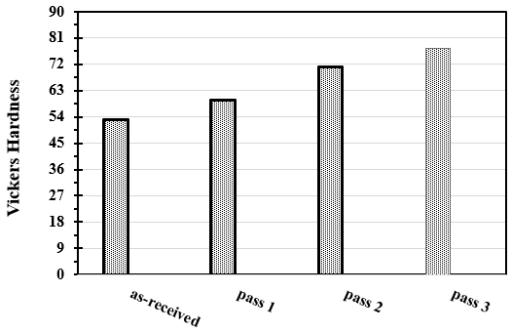

Fig. 10. Variations of hardness versus number of passes in the CGP process.

3.2. Forming limit diagrams and anisotropy

Fig. 11 shows the FLD for the as-received sample and CGP-processed samples. Major and minor strain points are shown, where blue and orange indicate the safe and fracture strain zones, respectively. It should be mentioned that the criterion used for identifying necking in FLD specimen was a sudden decrease in the load-stroke diagram. According to Fig. 11(b), formability decreased sharply in the first CGP pass compared to the as-received sample, for FLD_0, a reduction of about 50% is observed. Then, it was enhanced slightly and increased steadily after the first pass with the increase of the number of CGP passes, where it rose by 8% and 25% for the second and third passes, respectively (Figs. 11(c) and 11(d). The reduction in FLD is due to strain hardening which restricts the movement of dislocations [36]. The improvement of FLDs with increasing CGP passes can be attributed to the diminishing influence of strain hardening, grain refinement and the dominance of the grain refinement mechanism. In summary, the decrease in formability from the as-received to the first pass can be attributed to strain hardening and accumulated dislocations behind deformed grain boundaries. On the other hand, the increase in formability at higher CGP passes can be described by reduced strain hardening effects and enhanced grain refinement.

The FLD_0, mechanical properties, and anisotropy coefficients obtained for the Al-1050 samples are illustrated in Table 2, as a function of CGP passes and for as-received samples. Sheet metals generally exhibit a variation in mechanical properties depending on direction due to the forming processes. The variation in their plastic behavior is described by a characteristic called the anisotropy coefficient. The anisotropy coefficient (R) is determined by uniaxial tension tests on sheet samples and is defined by Eq. (5):

$$R = {\varepsilon_w}/{\varepsilon_t} \tag{5}$$

Where ε_w and ε_t are transverse direction (perpendicular to the rolling direction) and thickness direction strains, respectively, which are determined by Eqs. (6) and (7):

$$\varepsilon_w = \ln({w}/{w_0}) \tag{6}$$

$$\varepsilon_t = \ln({t}/{t_0}) \tag{7}$$

Where w, w_0, t, and t_0 represent the final width, initial width, final thickness and initial thickness, respectively. The anisotropy coefficient is equal to one for an isotropic material. The coefficient of normal anisotropy ($\bar{R}$) is the average of the R-values obtained for different directions in the plane of the sheet metal and is determined by:

$$\bar{R} = \frac{R_0 + 2R_{45} + R_{90}}{4} \tag{8}$$

Where R_0, R_{45}, and R_{90} are the R-values obtained in the longitudinal direction (rolling), transverse direction (perpendicular to the rolling direction) and 45°, respectively. Planar anisotropy is a measure of the variation of normal anisotropy with the angle to the rolling direction and is determined by the Eq. (9):

$$\Delta R = \frac{R_0 - 2R_{45} + R_{90}}{2} \tag{9}$$

The results of $\bar{R}$ and ΔR for as-received and the three different passes have been shown in Table 2. It shows that ΔR for the first pass decreased compared to the as-received sample by about 2.2%, however, it further dropped by up to 36% for the second pass. In the third pass, again a decree of about 5 times has been appeared compared to the second pass. For $\bar{R}$, there is a steady declining trend until the first pass, where it reached 0.441, with a 21% reduction compared to the as-received samples. However, after the first pass, there is an increase for the second and the third passes, with values

of 0.691 and 0.629, respectively. Table 2 also shows the n and k values for the as-received and different passes. The results demonstrated that the values of k increased as the number of passes went up compared to the as-received sample (with k = 79.15), where for the first, second and third passes, k was calculated as 235, 229 and 243.33, respectively. Moreover, the values of n are also shown in Table 2. The results revealed that n was reduced in the first pass compared to the as-received state (with n = 0.1977), then increased in the second and third passes. The findings demonstrate that the trend of the n-value closely aligns with the changes in formability. Initially, n decreases sharply after the first CGP pass but gradually transitions into an upward trend, a pattern that is similarly reflected in the FLD.

In order to validate the accuracy of the FLD tests, a deep drawing test was carried out on three-pass CGP-processed Al-1050 sheet samples using a punch with a flat head. The deep drawing test was conducted, and the resultant samples were obtained, as shown on Fig. 12(a).

Table 2. Mechanical properties, FLD_0, and anisotropy coefficients for the as-received sample and different CGP passes

Number of CGP passes	UTS (MPa)	YS (MPa)	Elongation (%)	FLD_0 (%)	n	k	$\bar{R}$	ΔR
As-received	147	118	20	24	0.1977	79.15	0.559	0.4065
Pass 1	185	133	11	12	0.1046	235	0.441	0.3976
Pass 2	178	140	13	13	0.1146	229.8	0.691	0.2545
Pass 3	177	160	13	16	0.1358	243.33	0.629	0.043

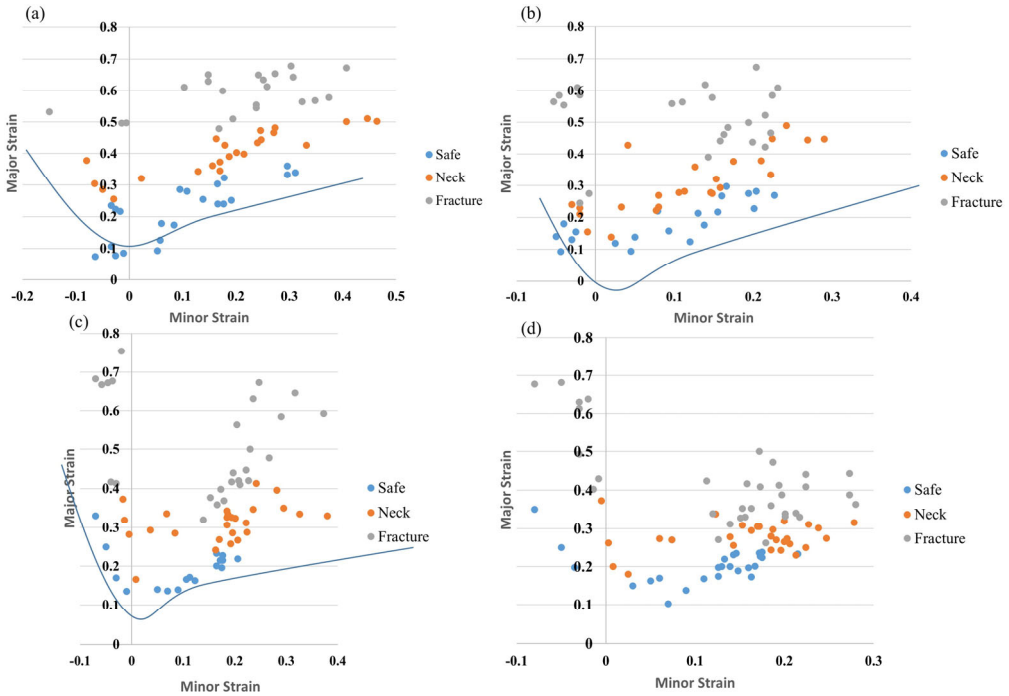

Fig. 11. FLD diagrams for the as-received and CGPed Al-1050 samples after various numbers of passes: (a) as-received, (b) pass 1, (c) pass 2, and (d) pass 3.

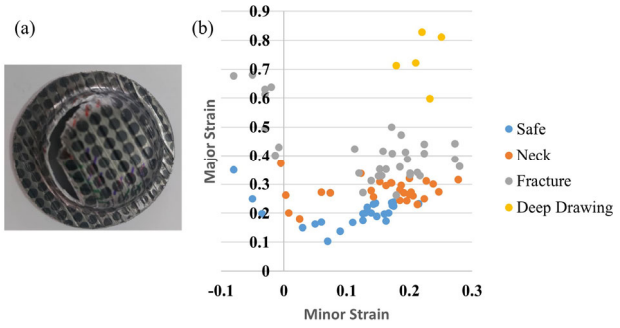

Fig. 12. (a) Sample achieved from deep drawing test, (b) major and minor strain values in the fractured zone of the sample plotted on the FLD diagram.

It is seen that the sample exhibits cracking in the regions near the punch radius. Moreover, the major and minor strains were measured for the samples and are shown in Fig. 12(b). It is shown that these points fall above the FLD curve, which validates the accuracy of the FLD results.

4. Conclusions

Due to the lack of studies considering FLD and anisotropy properties of Al-1050 for CGP-processed samples, this study aimed to investigate the CGP process for Al-1050. FLDs, mechanical properties and anisotropy coefficients were experimentally evaluated for CGPed samples. The key findings are summarized as follows:

- Compared to the as-received material, the yield strength of CGPed sample was enhanced and continued to increase with the number of passes. However, the ultimate tensile strength peaked at 185 MPa after the first pass (an 26% increase), and then decreased as the number of passes increased from one to three.
- Elongation decreased sharply after the first CGP pass compared to the as-received condition. However, with continued CGP processing, elongation improved. An 18% increase was observed for the second and third passes compared to the first pass.
- FLD results showed that formability dropped significantly after the first CGP pass, but subsequent passes led to continuous improvement, with increases of 8% and 25% for the second and third passes, respectively.
- The CGP process and increased number of passes significantly reduced the planar anisotropy.
- Hardness increased consistently with the number of CGP passes.
- The deep drawing test on CGP processed sheet metal confirmed the validity of the FLD results.

Conflict of interest

All authors confirm that there are no potential conflicts of interest related to the submission of this article.

Funding

The authors declare that they have no known competing financial interests or personal relationships that could have appeared to influence the work reported in this paper.

5. References

[1] Valiev, R. Z., Islamgaliev, R. K., & Alexandrov, I. V. (2000). Bulk nanostructured materials from severe plastic deformation. *Progress in Materials Science*, *45*(2), 103–189. https://doi.org/10.1016/S0079-6425(99)00007-9

[2] Valiev, R. Z., & Langdon, T. G. (2006). Principles of equal-channel angular pressing as a processing tool for grain refinement. *Progress in Materials Science, 51*(7), 881–981. https://doi.org/10.1016/j.pmatsci.2006.02.003

[3] Valiev, R. Z., Kozlov, E. V., Ivanov, Y. F., Lian, J., Nazarov, A. A., & Baudelet, B. (1994). Deformation behaviour of ultra-fine-grained copper. *Acta Metallurgica et Materialia*, *42*(7), 2467-2475. https://doi.org/10.1016/0956-7151(94)90326-3

[4] Mahmoodi, M., Tagimalek, H., Maraki, M. R., & Karimi, S. (2022). Experimental and numerical investigation of the formability of cross and accumulative roll bonded 1050 aluminum alloy sheets in single point incremental forming process. *International Journal of Engineering, 35*(9), 1707-1715. https://doi.org/10.5829/ije.2022.35.09C.05

[5] Huang, J., Zhu, Y. T., Alexander, D. J., Liao, X., Lowe, T. C., & Asaro, R. J. (2004). Development of repetitive corrugation and straightening. *Materials Science and Engineering A*, *371*(1-2), 35–39. https://doi.org/10.1016/S0921-5093(03)00114-X

[6] Lee, J. W., & Park, J. J. (2002). Numerical and experimental investigations of constrained groove pressing and rolling for grain refinement. *Journal of Materials Processing Technology, 130*, 208-213. https://doi.org/10.1016/S0924-0136(02)00722-7

[7] Mirsepasi, A., Nili-Ahmadabadi, M., Habibi-Parsa, M., Ghasemi-Nanesa, H., & Dizaji, A. F. (2012). Microstructure and mechanical behavior of martensitic steel severely deformed by the novel technique of repetitive corrugation and straightening by rolling. *Materials Science and Engineering A, 551*, 32-39. https://doi.org/10.1016/j.msea.2012.04.073

[8] Mishra, R. S., & Ma, Z. Y. (2005). Friction stir welding and processing. *Materials Science and Engineering: R: Reports, 50*(1-2), 1–78. https://doi.org/10.1016/j.mser.2005.07.001

[9] Richert, M., Liu, Q., & Hansen, N. (1999). Microstructural evolution over a large strain range in

aluminum deformed by cyclic-extrusion–compression. *Materials Science and Engineering A, 260*(1-2), 275-283. https://doi.org/10.1016/S0921-5093(98)00988-5

[10] Shin, D. H., Park, J. J., Kim, Y. S., & Park, K. T. (2002). Constrained groove pressing and its application to grain refinement of aluminum. *Materials Science and Engineering A, 328*(1-2), 98–103. https://doi.org/10.1016/S0921-5093(01)01665-3

[11] Tsuji, N., Saito, Y., Utsunomiya, H., & Tanigawa, S. (1999). Ultra-fine grained bulk steel produced by accumulative roll-bonding (ARB) process. *Scripta Materialia, 40*(7), 795–800. https://doi.org/10.1016/S1359-6462(99)00015-9

[12] Zhilyaev, A. P., & Langdon, T. G. (2008). Using high-pressure torsion for metal processing: fundamentals and applications. *Progress in Materials Science*, *53*(6), 893–979. https://doi.org/10.1016/j.pmatsci.2008.03.002

[13] Saito, Y., Tsuji, N., Utsunomiya, H., Sakai, T., & Hong, R. G. (1998). Ultra-fine grained bulk aluminum produced by accumulative roll-bonding (ARB) process. *Scripta Materialia*, *39*(9), 1221–1227. https://doi.org/10.1016/S1359-6462(98)00302-9

[14] Saito, Y., Utsunomiya, H., Tsuji, N., & Sakai, T. (1999). Novel ultra-high straining process for bulk materials—development of the accumulative roll-bonding (ARB) process. *Acta Materialia, 47*(2), 579–583. https://doi.org/10.1016/S1359-6454(98)00365-6

[15] Shin, D., Park, J., Kim, Y., & Park, K. (2002). Constrained groove pressing and its application to grain refinement of aluminum. *Materials Science and Engineering A, 328*(1-2), 98–103. https://doi.org/10.1016/S0921-5093(01)01665-3

[16] Khodabakhshi, F., Kazeminezhad, M., & Kokabi, A. H. (2010). Constrained groove pressing of low carbon steel: nano-structure and mechanical properties. *Materials Science and Engineering A, 527*(16-17), 4043–4049. https://doi.org/10.1016/j.msea.2010.03.005

[17] Krishnaiah, A., Chakkingal, U., & Venugopal, P. (2005). Production of ultrafine grain sizes in aluminium sheets by severe plastic deformation using the technique of groove pressing. *Scripta Materialia*, *52*(12), 1229–1233. https://doi.org/10.1016/j.scriptamat.2005.03.001

[18] Khakbaz, F., & Kazeminezhad, M. (2012). Work hardening and mechanical properties of severely deformed AA3003 by constrained groove pressing. *Journal of Manufacturing Processes, 14*(1), 20–25. https://doi.org/10.1016/j.jmapro.2011.07.001

[19] Khakbaz, F., & Kazeminezhad, M. (2012). Strain rate sensitivity and fracture behavior of severely deformed Al–Mn alloy sheets. *Materials Science and Engineering A, 532*, 26–30. https://doi.org/10.1016/j.msea.2011.10.057

[20] Krishnaiah, A., Chakkingal, U., & Venugopal, P. (2005). Applicability of the groove pressing technique for grain refinement in commercial purity copper. *Materials Science and Engineering A, 410*, 337–340. https://doi.org/10.1016/j.msea.2005.08.101

[21] Rafizadeh, E., Mani, A., & Kazeminezhad, M. (2009). The effects of intermediate and postannealing phenomena on the mechanical properties and microstructure of constrained groove pressed copper sheet. *Materials Science and Engineering A*, *515*(1-2), 162–168. https://doi.org/10.1016/j.msea.2009.03.081

[22] Satheesh Kumar, S. S., & Raghu, T. (2011). Tensile behavior and strain hardening characteristics of constrained groove pressed nickel sheets. *Materials and Design, 32*(8-9), 4650–4657. https://doi.org/10.1016/j.matdes.2011.03.081

[23] Khodabakhshi, F., & Kazeminezhad, M. (2011). The annealing phenomena and thermal stability of severely deformed steel sheet. *Materials Science and Engineering A, 528*(15), 5212–5218. https://doi.org/10.1016/j.msea.2011.03.024

[24] Khodabakhshi, F., & Kazeminezhad, M. (2011). The effect of constrained groove pressing on grain size, dislocation density and electrical resistivity of low carbon steel. *Materials and Design, 32*(6), 3280–3286. https://doi.org/10.1016/j.matdes.2011.02.032

[25] Ganjiani, M., & Assempour, A. (2007). The performance of karafillis-boyce yield function on determination of forming limit diagrams. *International Journal of Engineering, 20*(1), 55-66.

[26] Goodwin, G. M. (1968). Application of strain analysis to sheet metal forming problems in the press shop. *Sae Transactions,* 380-387. https://doi.org/10.4271/680093

[27] Marciniak, Z., & Kuczyński, K. (1967). Limit strains in the processes of stretch-forming sheet metal. *International Journal of Mechanical Sciences, 9*(9), 609-620. https://doi.org/10.1016/0020-7403(67)90066-5

[28] Zahedi, A., Dariani, B. M., & Mirnia, M. J. (2019). Experimental determination and numerical prediction of necking and fracture forming limit curves of laminated Al/Cu sheets using a damage plasticity model. *International Journal of Mechanical Sciences, 153*, 341-358. https://doi.org/10.1016/j.ijmecsci.2019.02.002

[29] Alizad Kamran, M., & Mollaei Dariani, B. (2022). Accuracy improvement of FLD prediction for anisotropic sheet metals using BBC 2008 advanced yield criterion. *Journal of the Brazilian Society of Mechanical Sciences and Engineering, 44*(10), 478-483. https://doi.org/10.1007/s40430-022-03770-x

[30] Lee, S., Saito, Y., Sakai, T., & Utsunomiya, H. (2002). Microstructures and mechanical properties of 6061 aluminum alloy processed by accumulative roll-bonding.

Materials Science and Engineering: A, 325(1-2), 228-235. https://doi.org/10.1016/S0921-5093(01)01416-2

[31] Mohamadi, V. (2019). *Effects of semi-constrained groove pressing on mechanical and microstructural properties of two-layer sheet* [Master's thesis, University of Zanjan].

[32] Khodabakhshi, F., Abbaszadeh, M. Eskandari, H., & Mohebpour, S. R. (2013). Application of CGP-cross route process for microstructure refinement and mechanical properties improvement in steel sheet. *Journal of Manufacturing Process, 15*(4), 533-541. https://doi.org/10.1016/j.jmapro.2013.08.001

[33] Hughes, D., & Hansen, N. (1997). High angle boundaries formed by grain subdivision mechanisms. *Acta Materialia, 45*(9), 3871-3886. https://doi.org/10.1016/S1359-6454(97)00027-X

[34] Alizadeh, M., & Samiei, M. (2014). Fabrication of nanostructured Al/Cu/Mn metallic multilayer composites by accumulative roll bonding process and investigation of their mechanical properties. *Materials & Design, 56*, 680-684. https://doi.org/10.1016/j.matdes.2013.11.067

[35] Wang, Y. M., & Ma, E. (2004). Three strategies to achieve uniform tensile deformation in a nanostructured metal. *Acta Materialia*, *52*(6), 1699-1709. https://doi.org/10.1016/j.actamat.2003.12.022

[36] Nie, N., Su, L., Deng, G., Li, H., Yu, H., & Tieu, A. K. (2021). A review on plastic deformation induced surface/interface roughness of sheet metallic materials. *Journal of Materials Research and Technology, 15*, 6574-6607. https://doi.org/10.1016/j.jmrt.2021.11.087